Desalination and Water Treatment
www.deswater.com

doi: 10.5004/dwt.2022.28327

255 (2022) 110–119
April

Fabrication of titanium dioxide/reduced graphene oxide nanofibers for photodegradation of tartrazine dye in aqueous solution

Mohammad Samir[a,b,*], Hamdy H. Hassan[a,c], Heba H. El-Maghrabi[d], Amr A. Nada[e,*]

[a]*Chemistry Department, Faculty of Science, Ain Shams University, Cairo, Egypt, Tel. +96565603845; email: mohammad.samir200@yahoo.com (M. Samir), Tel. +201115577356; email: hamdihh@sci.asu.edu.eg (H.H. Hassan)*
[b]*Research Sector, Chemistry Department, Faculty of Science, Kuwait University, Kuwait*
[c]*Faculty of Science, Galala University, New Galala City, 43511 Egypt*
[d]*Department of Refining, Egyptian Petroleum Research Institute, Cairo, 11727, Egypt, Tel. +201091816259; email: hebachem@yahoo.com (H.H. El-Maghrabi)*
[e]*Department of Analysis and Evaluation, Egyptian Petroleum Research Institute, Cairo 11727, Egypt, Tel. +201116560625; email: amr.nada@epri.sci.eg/chem_amr@yahoo.com (A.A. Nada)*

Received 12 June 2021; Accepted 12 January 2022

ABSTRACT

Titanium dioxide/reduced graphene oxide composite nanofibers were fabricated by electrospinning technique. The nanofibers have been prepared by optimizing the ratio of reduced graphene oxide (rGO) to titanium dioxide (TiO_2). The morphological, structural and optical properties have been studied by scanning electron microscopy, X-ray diffraction, Raman spectroscopy, and UV–Vis spectrophotometry. The surface area has been measured using Brunauer–Emmett–Teller method. The photocatalytic efficiency has been detected by the degradation of tartrazine dye under visible light. The results present that the degradation efficiency reaches 92% for the nanocomposite under visible light. However, the degradation efficiency was 10% for TiO_2 only. Moreover, the prepared nanofibers have acceptable stability for several times use. The high efficiency of prepared nanofibers is due to the presence of rGO which improves the photocatalytic activity of nanofibers to degradation of harmful pollutant in water.

Keywords: Tartrazine; Reduced graphene oxide; Titanium dioxide; Organic pollutant; Degradation; Water remediation

1. Introduction

Water is the main constituent of life on the earth. It is vital for all forms of life. At the same time, hazards resulting from water are considered to be very high for all living organisms due to the pollution that we cause [1,2]. Because of their toxic nature, organic dyes are part of the major contaminants of industrial wastewater [3–5]. One of these dyes is tartrazine, which is a synthetic lemon-yellow azo dye used to colour foods, pharmaceutical products, and cosmetics. It seems to cause many diseases and is responsible for some allergic and intolerance reactions [6,7]. Because of its high solubility in water, it is not easy to remove tartrazine from water. Several methods have been proposed for the removal of synthetic dyes like tartrazine from water, including biological treatment, physical adsorption, chemical and electrochemical oxidation, chemical coagulation and precipitation [8–15]. Nowadays, photocatalytic oxidation is considered to be one of the most attractive methods because of its efficiency, simple process equipment, easy to control operating conditions, availability of catalytic materials, and no secondary pollution [16–20]. Titanium dioxide is mainly used as a photocatalyst in the degradation of organic pollutants because

* Corresponding author.

of its high photocatalytic performance, long-term stability, availability, nontoxicity, and low cost, but at the same time, titanium dioxide has its disadvantages. First of these is the high recombination rate of photogenerated electrons and holes. The second disadvantage is its relatively wide-band gap (~3.2 eV) [21–23]. To overcome these challenges, a lot of research is focused on improving the photocatalytic properties of titanium dioxide (TiO_2). Scientists used different ways to emphasize this improvement, such as surface modification, dye sensitization and doping of TiO_2. The doping method includes metal doping such as Fe, Zn, Ag and Gd and non-metal doping such as nitrogen and carbon [24–31]. Carbon materials such as graphene oxide (GO) and reduced graphene oxide (rGO) are used for producing TiO_2-based photocatalysts, because they have large surface area, chemical stability, compatibility with various substrates, and easy processability [32]. At present, there are many research studies on coupling TiO_2 with one or more composites in order to improve the photocatalytic process [33–35]. For example, Vaiano et al. [36] prepared TiO_2-graphite composites (TiO_2-G) using different amounts of graphite powder (G). The UV–vis DRs showed an absorption in the visible light region for TiO_2-G composites, whereas the band-gap energy value did not change. The photocatalytic performance of TiO_2 and TiO_2-G photocatalysts has been evaluated in the degradation of paracetamol under UV light. The results showed a complete degradation of paracetamol after 120 min and about 88% removal of TOC after 180 min using TiO_2-G photocatalysts, evidencing an improvement in photocatalytic performance due to the presence of graphite in the composites if compared with bare TiO_2. Mugunthan et al. [37] synthesized a TiO_2–SnO_2 mixed-oxide catalyst with a different ratio of Ti to Sn and evaluated its photocatalytic performance in the degradation of diclofenac from wastewater under UV irradiation. The results showed that the catalytic activity of TiO_2 was enhanced by the addition of a small quantity of Sn. Also, it was noticed that the energy band gap of the prepared photocatalysts was increased by increasing Sn content. The most effective photocatalyst was the one with a molar ratio of 20:1. The result showed a complete mineralization of diclofenac with a maximum total organic carbon removal of 90% with repeatability and stability over the repeated reaction cycles. In this work we used electrospinning to synthesize one-dimensional (1-D) TiO_2 nanofibers decorated by two-dimensional (2-D) rGO to take advantage of both. The advantages of (1-D) TiO_2 nanofibers are the following: (1) they offer eased transport and collection of electrons because of the reduced number of trapping positions; (2) they assist enhanced light scattering toward the red part of the spectrum. But at the same time, they suffer from reduced internal surface area, which affects their performance, especially when used for degradation of organic pollutants [38]. We enhanced the surface area of (1-D) TiO_2 by interacting with the (2-D) structure of rGO. Also, this method will help us to reduce the band gap of TiO_2 to be active under visible light and increasing of stability between electron–hole pairs leads to improving the photocatalytic activities. The aim of this work is to prepare TiO_2/rGO nanocomposite in different ratios and study the structural, morphological, optical properties and their effects on degradation of tartrazine pollutant in water under visible light.

2. Experimental

2.1. Chemicals and materials

Graphite powder 99.5 wt.%, titanium(IV) isopropoxide 97%, polyvinylpyrrolidone (PVP; Mw = 1,300,000 g moL^{-1}), acetic acid (98%), absolute ethanol (99%), sodium nitrate 99 wt.%, potassium permanganate 98 wt.%, sulfuric acid 98% w/v, hydrogen peroxide 30% w/v, and tartrazine were purchased from Sigma-Aldrich. All purchased compounds are used as received, with no further purification.

2.2. Synthesis of graphene oxide

Graphene oxide was synthesized using Hummer method with graphite powder as starting material. The 1 g of graphite, 0.5 g of sodium nitrate and 23 mL of H_2SO_4 were mixed in a beaker for 10 min. Then, 3 g of $KMnO_4$ was gradually added to the mixture with stirring for 24 h. Then, 50 mL of distilled water was added, and the mixture was heated to 98°C for 30 min with stirring. Then 150 mL of distilled water and 60 mL of H_2O_2 were added to the mixture. Finally, the precipitate was washed several times by distilled water and dried at 60°C for 12 h [18,39–41].

2.3. Preparation of TiO_2/rGO nanofibers

rGO incorporated TiO_2 nanofibers with different ratio between rGO and TiO_2 were fabricated using the electrospinning technique. The spun solution has 3 mL of ethanol, 2 mL of acetic acid, 0.3 g of PVP and 1.5 mL of TTIP. The mixture was stirred for 1 h with different weight ratios of GO to TiO_2 to get TG0, TG1, TG2, TG3 and TG4 nanofibers, respectively. The spun solution was added in syringe with 10-gauge nozzle. The rate flow of solution was 5 mL h^{-1} under high voltage power (1.3 kV cm^{-1}) between the rotating collector and nozzle. The prepared nanofibers were calcined at 400°C for 3 h [42,43].

2.4. Characterization

The structure of prepared photocatalysts was confirmed using X-ray diffraction (XRD) (Shimadzu XD-1) utilizing Cu-Ka radiation (λ = 0.15406 nm). Raman test was carried out on the dispersive Raman microscope (Senterra, Bruker) instrument at a laser wavelength of 532 nm [doubled Nd:YAG laser (neodymium-doped yttrium aluminum garnet)] and power of 10 mW. The functional groups of prepared composite nanofibers were recognized using Fourier-transform infrared (FTIR) spectrometer (Perkin Elmer) with standard KBr pellets. The morphology of prepared composite nanofibers was recorded by a scanning electron microscopy (SEM, Quanta-250 FEG, FEI, The Netherlands). The UV–Vis–DR spectra were implemented through Jasco V-570 joined with a diffuse reflectance (DR) (Shimadzu IRS-2200). Specific surface area was measured from the N_2 adsorption–desorption isotherms at liquid nitrogen temperature (−196°C) using (Quantachrome Nova 3200 S) automates gas sorption apparatus. Prior to such measurements all samples

were perfectly degassed at 300°C for 6 h and under vacuum pressure 1.3 × 10^{-3} Pa.

2.5. Photocatalytic activity measurement

To evaluate the photocatalytic activity of the TiO_2/rGO composite NFs, we used tartrazine as a model of organic pollutant. The performance of photocatalyst was evaluated by analysing the decrease in concentration of the tartrazine during exposure to visible light radiation. The reaction temperature was preserved constant at 25°C ± 0.2°C during the entire experiment by circulating water around the photoreactor. The decomposition process was proceeded in sundry beakers containing a suspension of 40 mg of photocatalyst in 100 mL of tartrazine solution (50 mg L^{-1}). At a distance of 10 cm, the mixture was irradiated by a 500 W linear halogen lamp (the wavelength distribution was in visible region) under continuous stirring. The emission spectrum of the halogen lamp is in the range 420–600 nm [44]. At the beginning, the solution mixture was stirred magnetically for 30 min in the absence of light to achieve the adsorption–desorption equilibrium of tartrazine [5]. Then, the solution was exposed to visible light for 3 h. After 30, 60, 120 and 180 min, 4 mL of the solution mixture was taken out and centrifuged to expel the catalyst. Then, the supernatant was analysed by a UV/vis spectrometer. The absorbance spectra of tartrazine were recorded to measure the change in the concentration. The absorption band of tartrazine is around 430 nm [45]. The photocatalytic degradation efficiency has been calculated by Eq. (1):

$$\text{Degradation efficiency}\% = \frac{(C_0 - C)}{C_0} \times 100 \quad (1)$$

where C_0 and C are the initial concentration and the final concentration of tartrazine before and after photoirradiation, respectively [46].

3. Results and discussion

3.1. Structural and chemical characterization

The TiO_2/rGO NFs with different amounts of graphene oxide (TGX) where is X = 0, 1, 2, 3 and 4, were prepared by electrospinning of polymeric solution containing titanium precursor and graphene oxide sheets. The X-ray diffraction patterns of all prepared samples TG0, TG1, TG2, TG3 and TG4 nanofibers are presented in Fig. 1. The samples show diffraction peaks at 2θ (degree) equal to 25.5°, 38.1°, 48.1°, 54.1°, 55.3° and 62.9°, which correspond to the (101), (004), (200), (105), (211) and (204) miller index, respectively. All the peaks were matched with the database in JCPDS, No 01-084-1285 for anatase-TiO_2 [47]. It can be noticed that all the diffraction peaks for all composites (TG0, TG1, TG2, TG3 and TG4) perfectly matched together and with the standard TiO_2. This means that no traces of impurity phases were detected and no structural alteration after the reduction of graphene oxide [48]. We calculated the average crystallites size of powders using Debye Scherrer's equation [49]. The results are 10.1, 11.5, 14.2, 14.5 and13.9 nm for TG0, TG1, TG2, TG3 and TG4, respectively. The results revealed that

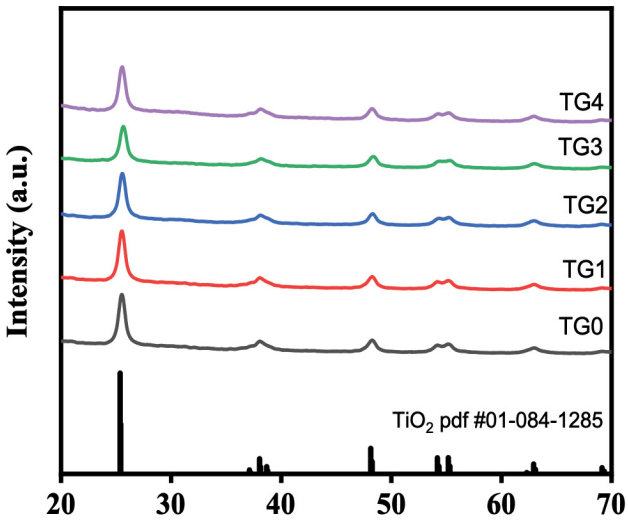

Fig. 1. XRD spectra of the samples TG0, TG1, TG2, TG3 and TG4 nanofibers.

the average size of TiO_2/rGO nanofibers crystallite increases slightly by increasing the rGO ratio compared to the pure TiO_2 nanofibers except for sample TG4. The decrease in crystallite size for sample TG4 may be attributed to the agglomeration of rGO sheets [50].

To confirm the quality of crystallite and the formation of TiO_2/rGO nanofibers, the Raman analysis was done, and the spectra were recorded in the range of 50–2000 cm^{-1}. Fig. 2 shows the Raman spectra of TG0, TG1, TG2, TG3 and TG4. We observed the characteristic peaks for all samples corresponding to the active mode of the anatase TiO_2 at 147.41 cm^{-1} (E_g), 198.17 cm^{-1} (E_g), 389.58 cm^{-1} (B_{1g}), 502.31 cm^{-1} (A_{1g} + B_{1g}) and 626.37 cm^{-1} (E_g) [38,51]. Also, the spectra of the composite TiO_2/rGO with different ratios showed the characteristic D and G band for GO at 1,337 and 1,578 cm^{-1} respectively. The D and G bands emphasize that the GO was introduced successfully into the nanofibers during electrospinning. The G band (1,578 cm^{-1}) is associated with in-plane stretching of the C–C bond, while the D band (1,337 cm^{-1}) is associated with basal plane defects in the structure [52]. The I_d/I_g ratio has been used to evaluate the reduction of GO. The I_d/I_g ratio for all samples, was 1.29, 1.29, 1.31 and 1.30 for TG1, TG2, TG3 and TG4, respectively. Since the Raman I_d/I_g ratio is inversely proportional to the average size of the sp^2 domains, the relatively high intensity of the I_d/I_g ratio indicates the presence of sp^3 defects within sp^2 during the reduction of GO and the high exfoliation of rGO layers. This emphasize that, a chemical bonding between TiO_2 and rGO was created by replacing of oxygen in GO by TiO_2 during reduction [18].

Formation of TiO_2/rGO nanofibers was confirmed by FTIR. In Fig. 3, the absorption band located at 450–900 cm^{-1} can be assigned to Ti–O bonding in TiO_2 nanofibers. It matched with previous results [42]. The band at 1,659 cm^{-1} is related to water –OH bending. The broad band at 3,455 cm^{-1} is due to the adsorbed water content in the surface of rGO and TiO_2. The bands at 1,728 cm^{-1} for C=O and at 1,386 cm^{-1} for C–OH indicate that TiO_2 binds to rGO at these sites [53–57].

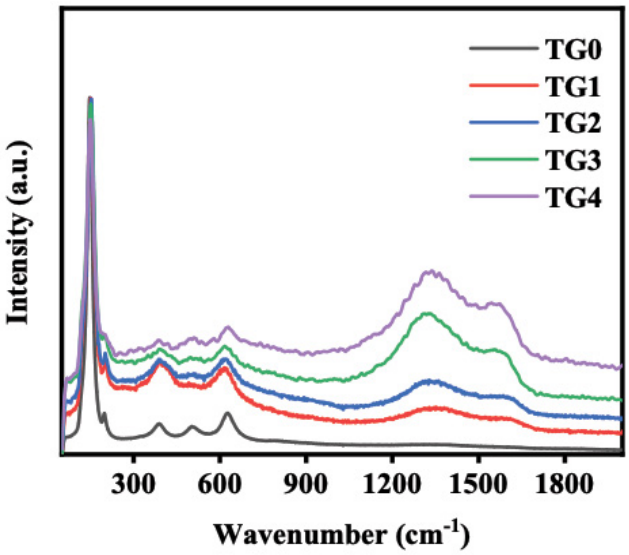

Fig. 2. Raman spectra of TG0, TG1, TG2, TG3 and TG4 nanofibers

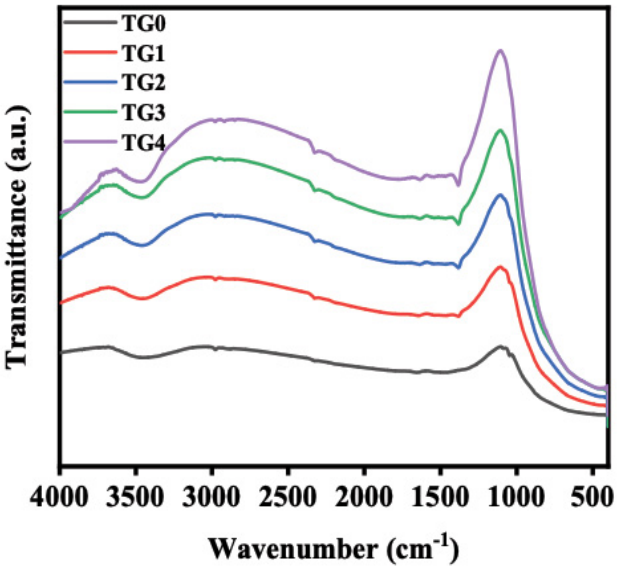

Fig. 3. FTIR for TG0, TG1, TG2, TG3 and TG4.

The morphology of TiO_2/rGO nanofibers has been studied using SEM. Fig. 4 presents the SEM images of the obtained TiO_2/rGO nanofibers after calcination. The formation of quite interconnected grid of nanofibers can be seen. In addition, wrinkles appear on the surface of the nanofibers indicating the presence of rGO sheets which increase by increasing rGO contents. The incorporation of rGO did not affect the nanofibrous morphology of TiO_2. By using the ImageJ, Java-based image processing software we measured average diameter of each sample. The results were (1.31 ± 0.21 μm), (1.82 ± 0.28 μm), (1.95 ± 0.31 μm), (2.23 ± 0.29 μm) and (2.25 ± 0.32 μm) for samples TG1, TG2, TG3 and TG4, respectively. It is obvious that the average diameter of the nanofibers increases with increasing rGO content. It may be attributed to the augmentation of the solution viscosity containing rGO in the electrospinning solution [5]. This increment manifests the successful incorporation of the reduced graphene oxide in the TiO_2 nanofibers.

As we discussed before, one of the challenges we are facing with TiO_2 is the reduced internal surface area. From Table 1 we can clearly notice increasing in surface area with increasing rGO content. The specific surface area varies between 15 and 72 m^2g^{-1}. It is well known that TiO_2 with large surface area has excellent photocatalytic activity as a result of providing more active adsorption sites and speed transport channels for large organic molecules [54].

The evaluation of the optical properties of titanium dioxide decorated by rGO was done by UV-Diffuse Reflectance Spectroscopy (UV–DRs). As presented in Fig. 5 the intensity of reflectance is decreasing gradually with increasing rGO from TG0 up to TG4. TG3 is the lowest intensity of reflectance that means it has the highest absorption of light in visible range. Upon increasing rGO content, considerable shifting of the reflectance edge toward a longer wavelength was observed. This red shift is due to the formation of Ti–O–C bond. The band gap of samples (E_g) was calculated and presented in Table 1. The decreasing in band gap from 3.1 to 2.9 eV with increasing rGO content confirms the improvement of optical properties of TiO_2 by rGO [58].

3.2. Photocatalytic performance

We used tartrazine as a paradigm for organic pollutants and evaluate photocatalytic activities of TiO_2/rGO nanofibers. The degradation of tartrazine by using TiO_2/rGO nanofibers with different amount of rGO under visible light (wavelength >400 nm) is shown in Fig. S1. It presents the UV−Vis absorbance spectra of tartrazine solution (major absorption band around 430 nm) at different time points 0, 30, 60, 120, and 180 min after storage in dark for 60 min and excluding the interference of adsorption. From Fig. 6a, it is clear that tartrazine under visible light in the absence of the photocatalyst is stable and hard to be photodegraded. After exposure to visible light for 180 min, tartrazine was degraded up to 92% in the presence of TiO_2/rGO nanofibers. Moreover, by increasing rGO contents, remarkably enhanced photocatalytic activities are shown, and tartrazine degradation increased from 10% for TG0 up to 92% for TG3. By further increasing rGO content in TG4, the photocatalytic activity decreased, and the tartrazine degradation was 78%. Whereas the photocatalytic activity is mainly controlled by light absorption capacity, crystalline phase, and separation efficiency of electron–hole pairs, the variation between the sample's efficiencies may be interpreted as follow: for the composites TG1, TG2 and TG3, with the rGO incorporation, the band gap energy decreases and the absorption edges are red shifted. In addition, the photoelectrons transferred quickly to the rGO layers, the probability of electron-hole recombination in TiO_2 is reduced. Moreover, more electrons will be available to participate in the photodegradation process, compared to the pure TiO_2 NFs. However, the use of an extra amount of rGO in TG4 reduces the light absorption on the TiO_2 surface, decreases the photoexcited electrons and increases the opportunity for the recombination of the photogenerated electron–hole pairs [5].

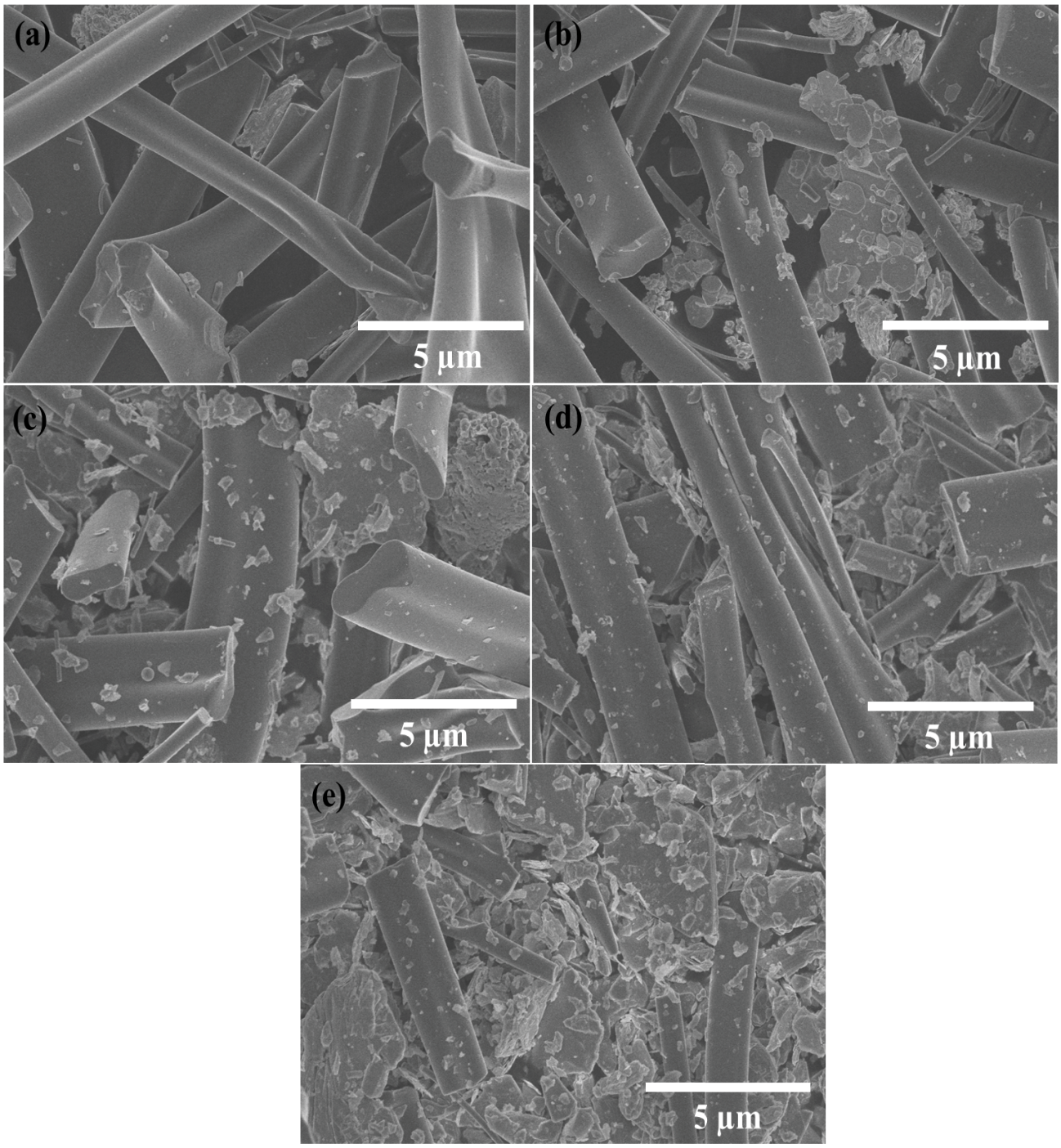

Fig. 4. SEM images for (a) TG0, (b) TG1, (c) TG2, (d) TG3 and (e) TG4.

Fig. 6b represents the degradation kinetic linear curves of tartrazine photodegradation by TiO_2/rGO nanofibers which were evaluated using a Langmuir–Hinshelwood first-order kinetics model [44,59]. The equation of the model can be expressed as

$$R = \frac{dC}{dT} = \frac{kKC}{\left(1 + KC\right)} \tag{2}$$

where R is the tartrazine degradation rate (mg L^{-1} min^{-1}), C is the concentration of tartrazine (mg L^{-1}), T is the irradiation time, k is the reaction rate constant (mg L^{-1} min^{-1}), and K is the adsorption coefficient (mg L^{-1}). The photodegradation reaction of tartrazine follows a pseudo-first-order kinetic [60]:

$$\ln\left(\frac{C_0}{C}\right) = kKT = k_a t \tag{3}$$

where k_a is the apparent first-order rate constant (min^{-1}) and C is the concentration at time t. k_a was calculated from the degradation kinetic linear curves (Fig. 6b) and recorded in Table 1. The results reveal that the rate constants are increasing in the following order: TG3 > TG2 > TG4 > TG1 > TG0. The rate constant shows a maximum of 0.0115 min^{-1} for TG3. It is obvious that the TiO_2/rGO nanofibers which produced by electrospinning have a higher photocatalytic activity under visible light, as proved by comparing with previous studies for degradation of tartrazine (Table 2).

For durability test, the nanofibers were recovered simply by filtering with filter paper, washed with deionized water and dried at 60°C. The reusability of the TG3 photocatalyst shown in Fig. 6c reveals that TG3 nanofibers have high stability after 5 cycles, and it recorded 88% degradation efficiency for tartrazine.

3.3. Photocatalytic mechanism

As we discussed before, TiO_2 nanofibers have a high band gap (3.2 eV) and a high recombination rate between electrons and holes. We enhanced it with rGO to decrease the band gap and increase the surface area, which will improve the photocatalytic activity. As shown in Fig. 7, when TG3 is exposed to visible light, it generates excited electrons and holes. The negatively charged electron migrates from the valance band to the conduction band, leaving behind positive charged holes. The photogenerated electrons react with the adsorbed water and oxygen to form hydroxyl (OH^-) and super oxide radicals ($^{\bullet}O_2^-$). By positive holes, the adsorbed hydroxyl ions and water molecules are oxidized to give hydroxyl radicals ($^{\bullet}OH$), which, in turn, degrade tartrazine to CO_2, H_2O and other harmless products [70,71].

Table 1
Brunauer–Emmett–Teller surface area, band gap, and kinetic parameters for TZ, TG0, TG1, TG2, TG3 and TG4

Sample	Surface area (±2 m^2g^{-1})	Band gap (eV)	k_a (min^{-1})	R^2
TZ	–	–	0.0001	0.91
TG0	15	3.18	0.0005	0.99
TG1	24	2.98	0.0021	0.99
TG2	40	2.91	0.0062	0.99
TG3	69	2.82	0.0115	0.99
TG4	72	2.95	0.0049	0.98

4. Conclusion

In conclusion, the study aimed to enhance the photocatalytic activity of (1-D) TiO_2 by interacting with the (2-D) structure of rGO. TiO_2/rGO nanofibers which were successfully prepared with different ratios between rGO and TiO_2 using the electrospinning technique. All samples were calcined at 400°C for 3 h. SEM images demonstrated that the average diameter of the nanofibers increased with increasing rGO content and confirmed

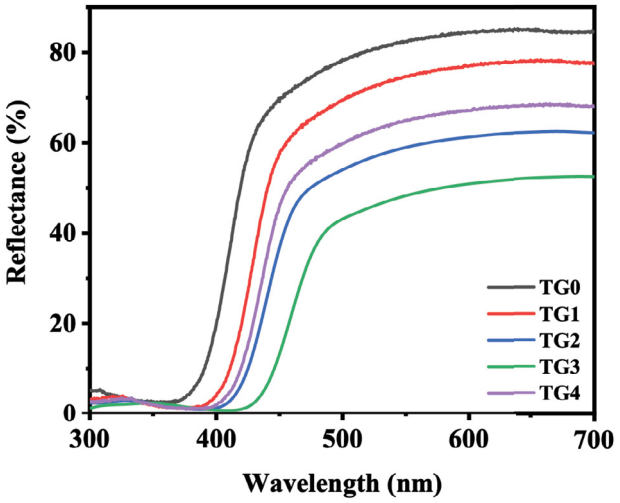

Fig. 5. UV–Vis diffuse reflectance spectra of the samples TG0, TG1, TG2, TG3 and TG4.

Table 2
Photocatalytic degradation of tartrazine dye in the presence of different photocatalyst materials

Photocatalyst	Radiation source	Catalyst loading (g L^{-1})	Degradation (%)	Time (min)	References
mpg-C_3N_4/Cu	UV	0.5	81.9	240	[61]
N-TiO_2/phosphors	Visible	3.0	85.0	90	[62]
Ni-CeO_2 NP	UV	1.0	65.4	360	[63]
Ni-CeO_2 NP	Visible	1.0	63.7	360	[63]
Straw sheaf – CuO	Visible	0.2	90.0	240	[64]
$LaFeO_3$/ZnO	UV	3.0	84.0	180	[65]
TiO_2	UV	0.5	78.0	360	[66]
CdS NP/PVP	Visible	0.2	85.0	540	[67]
Ag/TiO_2	UV	0.8	89.0	120	[68]
TiO_{2op}	UV	0.5	83.0	240	[69]
TiO_2/rGO NF	Visible	0.4	92.0	180	This work

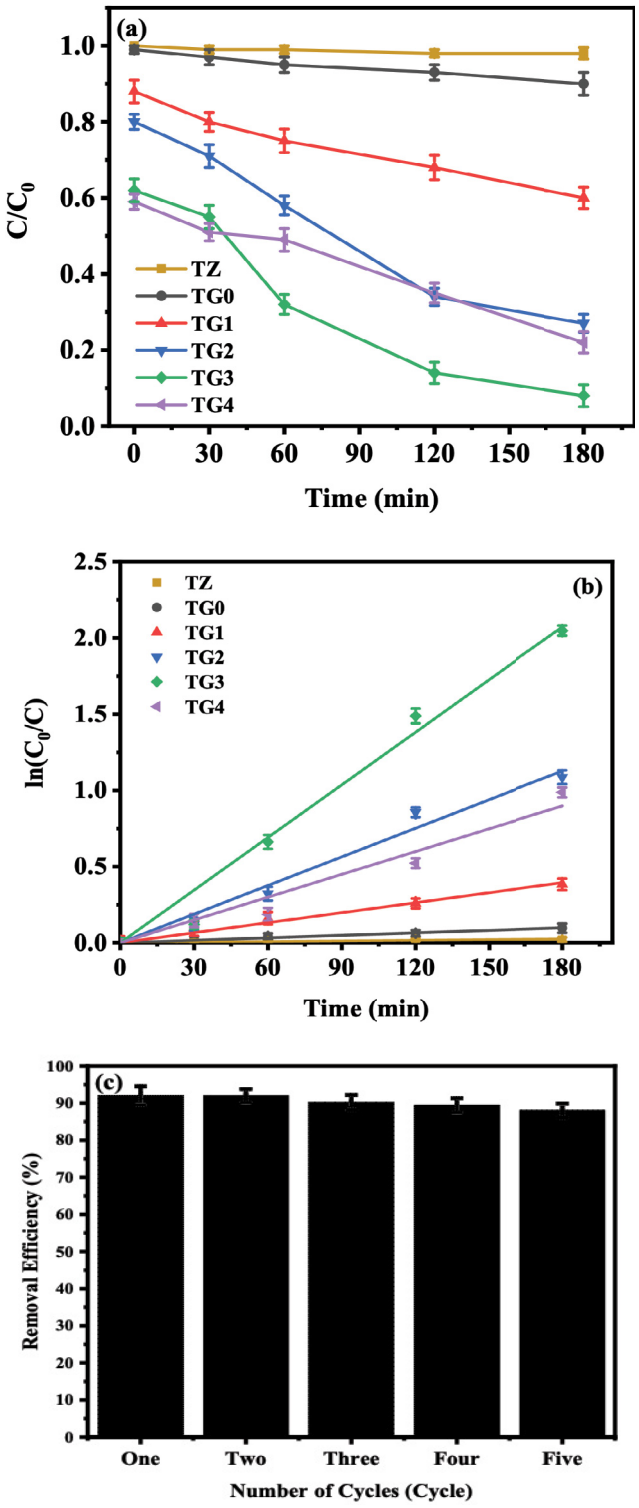

Fig. 6. (a) Photodegradation of tartrazine and (b) kinetic of tartrazine degradation by TZ, TG0, TG1, TG2, TG3 and TG4 and (c) photodegradation stability curve of tartrazine by TG3.

successful incorporation of the reduced graphene oxide into the TiO_2 nanofibers. FTIR and Raman confirmed the reduction of GO after calcination. XRD showed that the

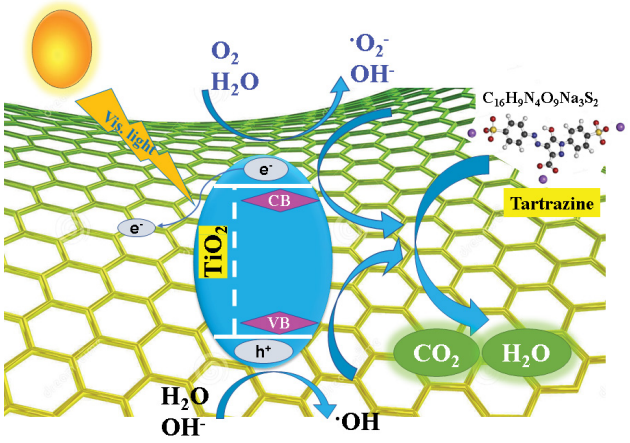

Fig. 7. Photocatalytic degradation mechanism of tartrazine on TG3 nanofibers.

successful introduction of rGO did not alter the structure of TiO_2. The specific surface area measurement showed a remarkable increase with increasing rGO content. UV–DRs clarified that the band gap energy of TiO_2/rGO NFs decreased from 3.19 to 2.95 eV because of the presence of rGO sheets. The combination of TiO_2 and rGO obviously increases the visible light photoresponse of TiO_2. TG3 shows the best photocatalytic activity for tartrazine degradation with 92% efficiency. By increasing the rGO content more in TG4, the efficiency of photocatalytic degradation decreased up to 78%, which is attributed to increasing the amount of rGO which reduces the light absorption on the TiO_2 surface and the photocatalytic efficiency of TiO_2/rGO nanofibers as well. Finally, we achieved our goal of preparing TiO_2/rGO nanofibers that could be used as photocatalysts in the degradation of several organic molecules under visible light, and we tested them on tartrazine dye with a 92% degradation efficiency. This study brings some insights into the potential of TiO_2/rGO Materials as promising and long-lasting catalysts for toxic organic dye reduction in wastewater and environment recovery.

References

[1] R.P. Schwarzenbach, T. Egli, T.B. Hofstetter, U. von Gunten, B. Wehrli, Global water pollution and human health, Annu. Rev. Environ. Resour., 35 (2010) 109–136.
[2] Q. Wang, Z. Yang, Industrial water pollution, water environment treatment, and health risks in China, Environ. Pollut., 218 (2016) 358–365.
[3] N. Arabzadeh, A. Khosravi, A. Mohammadi, N.M. Mahmoodi, Enhanced photodegradation of hazardous tartrazine by composite of nanomolecularly imprinted polymer-nanophotocatalyst with high efficiency, Desal. Water Treat., 57 (2016) 3142–3151.
[4] V.K. Gupta, R. Jain, A. Nayak, S. Agarwal, M. Shrivastava, Removal of the hazardous dye—tartrazine by photodegradation on titanium dioxide surface, Mater. Sci. Eng., C, 31 (2011) 1062–1067.
[5] M. Nasr, S. Balme, C. Eid, R. Habchi, P. Miele, M. Bechelany, Enhanced visible-light photocatalytic performance of electrospun rGO/TiO_2 composite nanofibers, J. Phys. Chem. C, 121 (2017) 261–269.

[6] P. Oancea, V. Meltzer, Kinetics of tartrazine photodegradation by UV/H_2O_2 in aqueous solution, Chem. Pap., 68 (2014) 105–111.
[7] S. Naama, T. Hadjersi, H. Menari, G. Nezzal, L. Baba Ahmed, S. Lamrani, Enhancement of the tartrazine photodegradation by modification of silicon nanowires with metal nanoparticles, Mater. Res. Bull., 76 (2016) 317–326.
[8] K.-i. Suehara, Y. Kawamoto, E. Fujii, J. Kohda, Y. Nakano, T. Yano, Biological treatment of wastewater discharged from biodiesel fuel production plant with alkali-catalyzed transesterification, J. Biosci. Bioeng., 100 (2005) 437–442.
[9] Y. Ji, Y. Wang, J. Sun, T. Yan, J. Li, T. Zhao, X. Yin, C. Sun, Enhancement of biological treatment of wastewater by magnetic field, Bioresour. Technol., 101 (2010) 8535–8540.
[10] J.M. Peralta-Hernández, C.A. Martínez-Huitle, J.L. Guzmán Mar, A. Hernández-Ramírez, Recent advances in the application of electro-Fenton and photoelectro-Fenton process for removal of synthetic dyes in wastewater treatment, J. Environ. Eng. Manage., 19 (2009) 257–265.
[11] P. Oancea, V. Meltzer, Photo-Fenton process for the degradation of Tartrazine (E102) in aqueous medium, J. Taiwan Inst. Chem. Eng., 44 (2013) 990–994.
[12] P.V. Nidheesh, M. Zhou, M.A. Oturan, An overview on the removal of synthetic dyes from water by electrochemical advanced oxidation processes, Chemosphere, 197 (2018) 210–227.
[13] S.S. Tahir, N. Rauf, Removal of a cationic dye from aqueous solutions by adsorption onto bentonite clay, Chemosphere, 63 (2006) 1842–1848.
[14] C.-Z. Liang, S.-P. Sun, F.-Y. Li, Y.-K. Ong, T.-S. Chung, Treatment of highly concentrated wastewater containing multiple synthetic dyes by a combined process of coagulation/flocculation and nanofiltration, J. Membr. Sci., 469 (2014) 306–315.
[15] M.-X. Zhu, L. Lee, H.-H. Wang, Z. Wang, Removal of an anionic dye by adsorption/precipitation processes using alkaline white mud, J. Hazard. Mater., 149 (2007) 735–741.
[16] J. Ménesi, L. Körösi, É. Bazsó, V. Zöllmer, A. Richardt, I. Dékány, Photocatalytic oxidation of organic pollutants on titania–clay composites, Chemosphere, 70 (2008) 538–542.
[17] Y. Zhou, Y. Qin, W. Dai, X. Luo, Highly efficient degradation of tartrazine with a benzoic acid/TiO_2 system, ACS Omega, 4 (2019) 546–554.
[18] A.A. Nada, H.R. Tantawy, M.A. Elsayed, M. Bechelany, M.E. Elmowafy, Elaboration of nano titania-magnetic reduced graphene oxide for degradation of tartrazine dye in aqueous solution, Solid State Sci., 78 (2018) 116–125.
[19] R. Elshypany, H. Selim, K. Zakaria, A.H. Moustafa, S.A. Sadeek, S.I. Sharaa, P. Raynaud, A.A. Nada, Magnetic ZnO crystal nanoparticle growth on reduced graphene oxide for enhanced photocatalytic performance under visible light irradiation, Molecules, 26 (2021) 2269, doi: 10.3390/molecules26082269.
[20] R. Ameta, S. Benjamin, A. Ameta, S.C. Ameta, Photocatalytic degradation of organic pollutants: a review, Mater. Sci. Forum, 734 (2013) 247–272.
[21] X. Yu, D. Lin, P. Li, Z. Su, Recent advances in the synthesis and energy applications of TiO_2-graphene nanohybrids, Sol. Energy Mater. Sol. Cells, 172 (2017) 252–269.
[22] M. Ates, Y. Bayrak, H. Ozkan, O. Yoruk, M. Yildirim, O. Kuzgun, Synthesis of rGO/TiO_2/PEDOT nanocomposites, supercapacitor device performances and equivalent electrical circuit models, J. Polym. Res., 49 (2019) 1–16, doi: 10.1007/s10965-018-1692-2.
[23] A. Petrella, G. Mascolo, S. Murgolo, V. Petruzzelli, E. Ranieri, D. Spasiano, D. Petruzzelli, Photocatalytic oxidation of organic micro-pollutants: pilot plant investigation and mechanistic aspects of the degradation reaction, Chem. Eng. Commun., 203 (2016) 1298–1307.
[24] S. Anandan, Y. Ikuma, K. Niwa, An overview of semi-conductor photocatalysis: modification of TiO_2 nanomaterials, Solid State Phenom., 162 (2010) 239–260.
[25] H. Zangeneh, A.A.L. Zinatizadeh, M. Habibi, M. Akia, M. Hasnain Isa, Photocatalytic oxidation of organic dyes and pollutants in wastewater using different modified titanium dioxides: a comparative review, J. Ind. Eng. Chem., 26 (2015) 1–36.
[26] Y.L. Pang, S. Lim, H.C. Yap, A.Z. Abdullah, Sonocatalytic degradation of Rhodamine B in the presence of iron-doped TiO_2 nanotubes: characterizations and reaction kinetic studies, AIP Conf. Proc., 1828 (2017) 020010, doi: 10.1063/1.4979381.
[27] S. Xiao, L. Zhao, X. Leng, X. Lang, J. Lian, Synthesis of amorphous TiO_2 modified ZnO nanorod film with enhanced photocatalytic properties, Appl. Surf. Sci., 299 (2014) 97–104.
[28] B. Jin, X. Zhou, J. Luo, X. Xu, L. Ma, D. Huang, Z. Shao, Z. Luo, Fabrication and characterization of high efficiency and stable Ag_3PO_4/TiO_2 nanowire array heterostructure photoelectrodes for the degradation of methyl orange under visible light irradiation, RSC Adv., 5 (2015) 48118–48123.
[29] M. Farbod, M. Kajbafvala, Effect of nanoparticle surface modification on the adsorption-enhanced photocatalysis of Gd/TiO_2 nanocomposite, Powder Technol., 239 (2013) 434–440.
[30] Y. Cao, Y. Yu, P. Zhang, L. Zhang, T. He, Y. Cao, An enhanced visible-light photocatalytic activity of TiO_2 by nitrogen and nickel-chlorine modification, Sep. Purif. Technol., 104 (2013) 256–262.
[31] W. Wei, C. Yu, Q. Zhao, G. Li, Y. Wan, Improvement of the visible-light photocatalytic performance of TiO_2 by carbon mesostructures, Chem. – A Eur. J., 19 (2013) 566–577.
[32] S. Sheshmani, M. Nayebi, Modification of TiO_2 with graphene oxide and reduced graphene oxide; enhancing photocatalytic activity of TiO_2 for removal of remazol Black B, Polym. Compos., 40 (2019) 210–216.
[33] D. Chen, Y. Cheng, N. Zhou, P. Chen, Y. Wang, K. Li, S. Huo, P. Cheng, P. Peng, R. Zhang, L. Wang, H. Liu, Y. Liu, R. Ruan, Photocatalytic degradation of organic pollutants using TiO_2-based photocatalysts: A review, Journal of Cleaner Production. 268 (2020) 121725.
[34] D.S. Pattanayak, J. Mishra, J. Nanda, P.K. Sahoo, R. Kumar, N.K. Sahoo, Photocatalytic degradation of cyanide using polyurethane foam immobilized Fe-TCPP-S-TiO_2-rGO nanocomposite, J. Environ. Manage., 297 (2021) 113312, doi: 10.1016/j.jenvman.2021.113312.
[35] W. Li, Y. Zuo, L. Jiang, D. Yao, Z. Chen, G. He, H. Chen, $Bi_2Ti_2O_7$/TiO_2/RGO composite for the simulated sunlight-driven photocatalytic degradation of ciprofloxacin, Mater. Chem. Phys., 256 (2020) 123650, doi: 10.1016/j.matchemphys.2020.123650.
[36] V. Vaiano, O. Sacco, M. Matarangolo, Photocatalytic degradation of paracetamol under UV irradiation using TiO_2-graphite composites, Catal. Today, 315 (2018) 230–236.
[37] E. Mugunthan, M.B. Saidutta, P.E. Jagadeeshbabu, Photocatalytic degradation of diclofenac using TiO_2-SnO_2 mixed oxide catalysts, Environ. Technol., 40 (2019) 929–941.
[38] G.S. Anjusree, T.G. Deepak, K.R. Narendra Pai, J. Joseph, T.A. Arun, S.V. Nair, A. Sreekumaran Nair, TiO_2 nanoparticles@TiO_2 nanofibers-an innovative one-dimensional material for dye-sensitized solar cells, RSC Adv., 4 (2014) 22941–22945.
[39] J. Chen, B. Yao, C. Li, G. Shi, An improved Hummers method for eco-friendly synthesis of graphene oxide, Carbon, 64 (2013) 225–229.
[40] H. Yu, B. Zhang, C. Bulin, R. Li, R. Xing, High-efficient synthesis of graphene oxide based on improved hummers method, Sci. Rep., 6 (2016) 36143, doi: 10.1038/srep36143.
[41] S. William, J. Hummers, R.E. Offeman, Preparation of graphitic oxide, J. Am. Chem. Soc., 80 (1958) 1339.
[42] A.A. Nada, M.F. Bekheet, R. Viter, P. Miele, S. Roualdes, M. Bechelany, BN/$Gd_xTi_{(1-x)}O_{(4-x)/2}$ nanofibers for enhanced photocatalytic hydrogen production under visible light, Appl. Catal., B, 251 (2019) 76–86.
[43] H.H. El-Maghrabi, A.A. Nada, M.F. Bekheet, S. Roualdes, W. Riedel, I. Iatsunskyi, E. Coy, A. Gurlo, M. Bechelany, Coaxial nanofibers of nickel/gadolinium oxide/nickel oxide as highly effective electrocatalysts for hydrogen evolution reaction, J. Colloid Interface Sci., 587 (2021) 457–466.
[44] A.A. Nada, M. Nasr, R. Viter, P. Miele, S. Roualdes, M. Bechelany, Mesoporous $ZnFe_2O_4$@TiO_2 nanofibers prepared by electrospinning coupled to PECVD as highly performing

photocatalytic materials, J. Phys. Chem., C, 121 (2017) 24669–24677.
[45] E. Gilpavas, C.M. Gómez, J.M. Rynkowski, I. Dobrosz-Gómez, M.Á. Gómez-García, Decolorization and mineralization of yellow 5 (E102) by UV/Fe^{2+}/H_2O_2 process. Optimization of the operational conditions by response surface methodology, C.R. Chim., 18 (2015) 1152–1160.
[46] S. Sugi, P. Usha Rajalakshmi, J. Shanthi, Photocatalytic degradation efficiency of $Cu_XZn_{1-X}O$ composite, Optik, 131 (2017) 406–413.
[47] H. Bao, S. Zhu, L. Zhou, H. Fu, H. Zhang, W. Cai, Mars–van-Krevelen mechanism-based blackening of nano-sized white semiconducting oxides for synergetic solar photo-thermocatalytic degradation of dye pollutants, Nanoscale, 12 (2020) 4030–4039.
[48] T. Xian, H. Yang, L. Di, J. Ma, H. Zhang, J. Dai, Photocatalytic reduction synthesis of $SrTiO_3$-graphene nanocomposites and their enhanced photocatalytic activity, Nanoscale Res. Lett., 9 (2014) 327, doi: 10.1186/1556-276X-9-327.
[49] H. Jensen, J.H. Pedersen, J.E. Jørgensen, J. Skov Pedersen, K.D. Joensen, S.B. Iversen, E.G. Søgaard, Determination of size distributions in nanosized powders by TEM, XRD, and SAXS, J. Exp. Nanosci., 1 (2007) 355–373.
[50] A.T. Habte, D.W. Ayele, Synthesis and characterization of reduced graphene oxide (rGO) started from graphene oxide (GO) using the tour method with different parameters, Adv. Mater. Sci. Eng., 2019 (2019) 5058163, doi: 10.1155/2019/5058163.
[51] M.C. Mathpal, A.K. Tripathi, M.K. Singh, S.P. Gairola, S.N. Pandey, A. Agarwal, Effect of annealing temperature on Raman spectra of TiO_2 nanoparticles, Chem. Phys. Lett., 555 (2013) 182–186.
[52] A. Radoń, P. Włodarczyk, D. Łukowiec, Structure, temperature and frequency dependent electrical conductivity of oxidized and reduced electrochemically exfoliated graphite, Physica E, 99 (2018) 82–90.
[53] M. Ruidíaz-Martínez, M.A. Álvarez, M.V. López-Ramón, G. Cruz-Quesada, J. Rivera-Utrilla, M. Sánchez-Polo, Hydrothermal synthesis of RGO-TiO_2 composites as high-performance UV photocatalysts for ethylparaben degradation, Catalysts, 10 (2020) 520, doi: 10.3390/catal10050520.
[54] S. Zhang, J. Xu, J. Hu, C. Cui, H. Liu, Interfacial growth of TiO_2-rGO composite by pickering emulsion for photocatalytic degradation, Langmuir, 33 (2017) 5015–5024.
[55] X. Bai, X. Zhang, Z. Hua, W. Ma, Z. Dai, X. Huang, H. Gu, Uniformly distributed anatase TiO_2 nanoparticles on graphene: synthesis, characterization, and photocatalytic application, J. Alloys Compd., 599 (2014) 10–18.
[56] P. Wang, J. Wang, X. Wang, H. Yu, J. Yu, M. Lei, Y. Wang, One-step synthesis of easy-recycling TiO_2-rGO nanocomposite photocatalysts with enhanced photocatalytic activity, Appl. Catal., B, 132–133 (2013) 452–459.
[57] N. Ibrayev, A. Zhumabekov, S. Ghyngazov, E. Lysenko, Synthesis and study of the properties of nanocomposite materials TiO_2-GO and TiO_2-rGO, Mater. Res. Express, 6 (2019) 125036.
[58] H. Zhang, X. Wang, N. Li, J. Xia, Q. Meng, J. Ding, J. Lu, Synthesis and characterization of TiO_2/graphene oxide nanocomposites for photoreduction of heavy metal ions in reverse osmosis concentrate, RSC Adv., 8 (2018) 34241–34251.
[59] K. Vasanth Kumar, K. Porkodi, A. Selvaganapathi, Constrain in solving Langmuir–Hinshelwood kinetic expression for the photocatalytic degradation of Auramine O aqueous solutions by ZnO catalyst, Dyes Pigm., 75 (2007) 246–249.
[60] A.S. Morshedy, H.R. Ali, A.A. Nada, A.M. Rabie, H.H. El-Maghrabi, Highly efficient imprinted polymer nano-composites for photocatalytic desulfurization of real diesel fuel, Environ. Technol. Innovation, 21 (2021) 101206, doi: 10.1016/j.eti.2020.101206.
[61] T. Zhang, I.P.A.F. Souza, J. Xu, V.C. Almeida, T. Asefa, Mesoporous graphitic carbon nitrides decorated with Cu nanoparticles: efficient photocatalysts for degradation of tartrazine yellow dye, Nanomaterials, 8 (2018) 636, doi: 10.3390/nano8090636.
[62] V. Vaiano, O. Sacco, G. Iervolino, D. Sannino, P. Ciambelli, R. Liguori, E. Bezzeccheri, A. Rubino, Enhanced visible light photocatalytic activity by up-conversion phosphors modified N-doped TiO_2, Appl. Catal., B, 176–177 (2015) 594–600.
[63] S.R. Ali, R. Kumar, S.K. Kadabinakatti, M.C. Arya, Enhanced UV and visible light—driven photocatalytic degradation of tartrazine by nickel-doped cerium oxide nanoparticles, Mater. Res. Express, 6 (2018) 25513, doi: 10.1088/2053-1591/aaee44.
[64] M.P. Rao, J.J. Wu, A.M. Asiri, S. Anandan, Photocatalytic degradation of tartrazine dye using CuO straw-sheaf-like nanostructures, Water Sci. Technol., 75 (2017) 1421–1430.
[65] V. Vaiano, G. Iervolino, D. Sannino, Photocatalytic removal of tartrazine dye from aqueous samples on $LaFeO_3$/ZnO photocatalysts, Chem. Eng. Trans., 52 (2016) 847–852.
[66] S.K. Al-Dawery, Photo-catalyst degradation of tartrazine compound in wastewater using TiO_2 and UV light, J. Eng. Sci. Technol., 8 (2013) 683–691.
[67] M. Darwish, A. Mohammadi, N. Assi, Microwave-assisted polyol synthesis and characterization of PVP-capped CDS nanoparticles for the photocatalytic degradation of tartrazine, Mater. Res. Bull., 74 (2016) 387–396.
[68] A. Jodat, A. Jodat, Photocatalytic degradation of chloramphenicol and tartrazine using Ag/TiO_2 nanoparticles, Desal. Water Treat., 52 (2014) 2668–2677.
[69] I.P.A.F. Souza, L.H.S. Crespo, L. Spessato, S.A.R. Melo, A.F. Martins, A.L. Cazetta, V.C. Almeida, Optimization of thermal conditions of sol-gel method for synthesis of TiO_2 using RSM and its influence on photodegradation of tartrazine yellow dye, J. Environ. Chem. Eng., 9 (2021) 104753, doi: 10.1016/j.jece.2020.104753.
[70] S. Chowdhury, R. Balasubramanian, Graphene/semiconductor nanocomposites (GSNs) for heterogeneous photocatalytic decolorization of wastewaters contaminated with synthetic dyes: a review, Appl. Catal., B, 160–161 (2014) 307–324.
[71] A. Tayel, A.R. Ramadan, O.A. El Seoud, Titanium dioxide/graphene and titanium dioxide/graphene oxide nanocomposites: synthesis, characterization and photocatalytic applications for water decontamination, Catalysts, 8 (2018) 491, doi: 10.3390/catal8110491.

Supplementary information

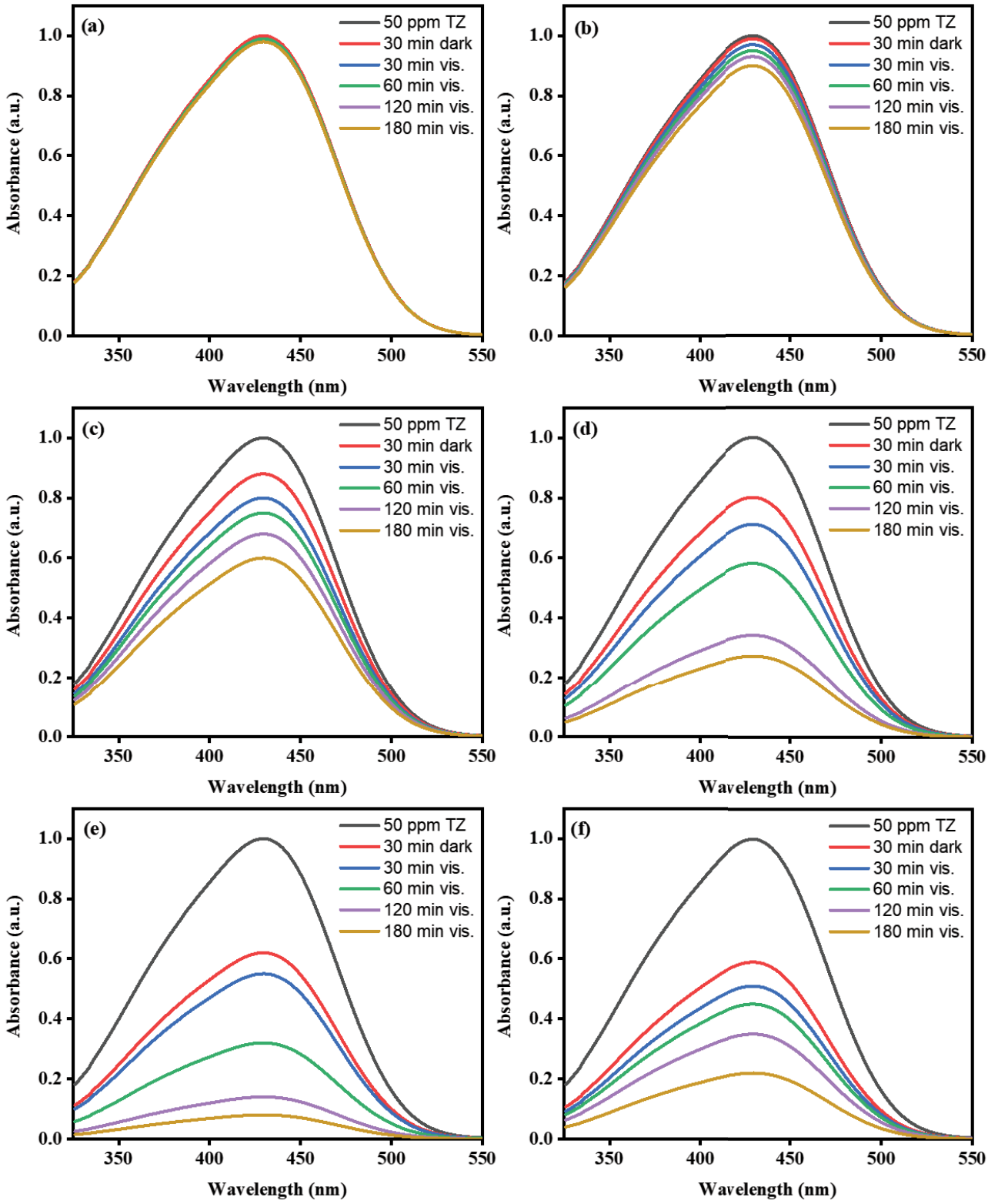

Fig. S1. (a) Tartrazine without catalyst, (b) TG0, (c) TG1, (d) TG2, (e) TG3 and (f) TG4.